Journal of Marine Science and Technology

Volume 26 | Issue 5 Article 12

NUMERICAL SIMULATION AND EXPERIMENTAL VALIDATION OF THE VIBRATION SUPPRESSION CONTROL BY USING INPUT SHAPING TECHNIQUE WITH EXTENDED KALMAN FILTER

Yi-Cheng Huang
Department of Mechatronics Engineering, National Changhua University of Education. Changhua, Taiwan, R.O.C., ychuang@cc.ncue.edu.tw

Yen-Lin Lee
Department of Mechatronics Engineering, National Changhua University of Education. Changhua, Taiwan, R.O.C.

Ming-You Ma
Department of Mechatronics Engineering, National Changhua University of Education. Changhua, Taiwan, R.O.C.

Recommended Citation

Huang, Yi-Cheng; Lee, Yen-Lin; and Ma, Ming-You (2018) "NUMERICAL SIMULATION AND EXPERIMENTAL VALIDATION OF THE VIBRATION SUPPRESSION CONTROL BY USING INPUT SHAPING TECHNIQUE WITH EXTENDED KALMAN FILTER," *Journal of Marine Science and Technology*: Vol. 26: Iss. 5, Article 12.
DOI: 10.6119/JMST.201810_26(5).0012
Available at: https://jmstt.ntou.edu.tw/journal/vol26/iss5/12

NUMERICAL SIMULATION AND EXPERIMENTAL VALIDATION OF THE VIBRATION SUPPRESSION CONTROL BY USING INPUT SHAPING TECHNIQUE WITH EXTENDED KALMAN FILTER

Acknowledgements

The financial support from Ministry of Science and Technology under Grant No. MOST 105-2221-E-018-006 is gratefully acknowledged.

Journal of Marine Science and Technology, Vol. 26, No. 5, pp. 731-742 (2018)
DOI: 10.6119/JMST.201810_26(5).0012

NUMERICAL SIMULATION AND EXPERIMENTAL VALIDATION OF THE VIBRATION SUPPRESSION CONTROL BY USING INPUT SHAPING TECHNIQUE WITH EXTENDED KALMAN FILTER

Yi-Cheng Huang, Yen-Lin Lee, and Ming-You Ma

Key words: damping ratio, extended Kalman filter, input shaping, vibration suppression.

ABSTRACT

The development of high-speed and high-precision machine tools is a challenge for designers because of the difficulties associated with the vibration control of mechanical systems. This study proposed a method to suppress such vibration by using input shaping functions with an extended Kalman filter (EKF). Input shaping is a technique that deploys one or several designed impulses to eliminate the vibration response of a mechanical system. To determine the parameters of an input shaper, the vibration of the mechanical system was assumed to be a simple, exponentially decaying sinusoidal signal. The EKF was used to estimate signal parameters, namely frequency and damping factors. The simulation and experimental results indicate that three input shaping functions with parameters can suppress vibration. Of the studied input shaping functions, a function with more impulses exhibited improved reduction in maximum vibration amplitude, whereas a zero vibration function exhibited the shortest settling time. A zero-voltage-derivative-derivative input shaping function provided the maximum damping effect.

I. INTRODUCTION

High speed and precision are fundamental requirements for the development of high-performance machine tools. However, challenges such as increase in acceleration magnitude and the effect of jerk (i.e., discontinuity in acceleration) are encountered when designing a high-speed feed system. If dynamic loading is induced in a system with a large inertia, the structure is more likely to be excited by loading with larger frequency bandwidth. A controller that can manage more vibration modes for suppressing structural vibration must be designed. For example, a uniaxial feed system with a ball screw can be excited in vibration with two or more natural modes because numerous mass blocks and elastic supports are present in this mechanical system. Moreover, because a linear motor is employed in the high-speed feed drive system and the supported system has low rigidity or the machined part has low stiffness, the controller must suppress the vibration that occurs at different frequencies and damping ratios, particularly under high acceleration motion with possible jerks.

Engineering technology evolves through collaboration between different disciplines. Singer and Seering (1990, 1994) proposed an input shaping technique that could be applied to any arbitrary trajectory for eliminating unwanted harmonics of a residual vibration error. Longman et al. (2013) proposed a synergetic approach for manufacturing a system design by simultaneously considering mechanism design and control system design. For example, when designing a cam driving mechanism, the constant rotational speed of a driving cam is generally assumed with an ideal control system. However, a sudden change in the resistance or inertia of the driven system can induce an associated change in the driving cam speed. Consequently, system motion is disturbed, and the required precision is compromised. However, the implementation of an intelligent controller with techniques, such as iterative learning control (ILC) and repetitive control techniques, can compensate for periodic errors. Similarly, for a cam defect in manufacturing, implementing intelligent control through software programming to overcome hardware imperfection and driving the cam to output the desired motion ensures the precision of the system for high-speed operation. This approach constitutes the fundamental principle of the input shaping technique.

Since the ILC was first developed in 1985, the intelligent selection of filtering bandwidth in a system with multiple natural

Paper submitted 05/04/18; revised 07/05/18; accepted 09/14/18. Author for correspondence: Yi-Cheng Huang (e-mail: ychuang@cc.ncue.edu.tw).
Department of Mechatronics Engineering, National Changhua University of Education. Changhua, Taiwan, R.O.C.

frequencies has never been addressed (Huang, 2015). An intelligent control system first compensates for the error because of a low frequency span. The control system then concentrates on the compensation of a dynamic error in high frequency. This intelligent bandwidth tuning by adjusting the filter bandwidth from a lower to higher frequency span first compensates for the geometric error and then reduces the dynamic error. Nuchkrua and Chen (2017) recently employed the command-based ILC to compensate for the equivalent geometric error of machine tools and extended its application to the trajectory optimization of robots. The pursuit on the trajectory tracing precision or trajectory planning optimization of robot was consistent with the underlining mechanism of input morphing in the ILC. The morphing input approach by Huang (2015) is similar to the input shaping proposed by Singer and Seering (1994). This input shaping approach was employed in the dynamic control of the feed system of machine tools (Singer, 1988; Tsai, 2017). Singer (1988) employed command shaping techniques for eliminating vibration and compensating for the contour error in a high-speed five-axis machine tool. To determine the time duration and amplitudes of impulses, the input shaper with the extended Kalman filter (EKF) was used in (Yoon, 2015). The online detection of parameters of a ring-down signal with the EKF was developed by Yazdanian (2015). Moreover, an approach combining the EKF and input shaping with zero vibration (ZV)/zero vibration derivative (ZVD) was studied to shape a dynamic system response in Yoon (2015).

II. THEORETICAL FORMULATION

1. Input Shaping Technique

Fig. 1 presents the schematic of an input shaping technique in the vibration control of a structural system. In this approach, two impulse responses are generated at two discrete instants, which can eliminate the subsequent vibrational displacement. This is termed a ZV approach. When the ZV approach was applied for vibration suppression in machine tools, its control stability was not satisfactorily robust. Therefore, the incorporation of a ZVD and ZVD-derivative (ZVDD) was employed in input shaping designs (Singer, 1988; Yoon, 2015; Tsai, 2017).

Assume that the original unshaped input to the feed system of a machine tool is $r(t)$. To suppress vibration from the combined responses of several system modes, the input command $r(t)$ should be modified. If two input shaping functions at two instants are selected, the corresponding equation can be written as follows:

$$InShp(t) = A_1\delta(t) + A_2\delta(t - t_2) \tag{1}$$

The resultant input shaping function can be expressed as follows:

$$\begin{aligned} r_{shape}(t) &= r_{shape,1}(t) + r_{shape,2}(t) \\ &= A_1 r(t) + A_2 r(t - t_2)u(t - t_2) \end{aligned} \tag{2}$$

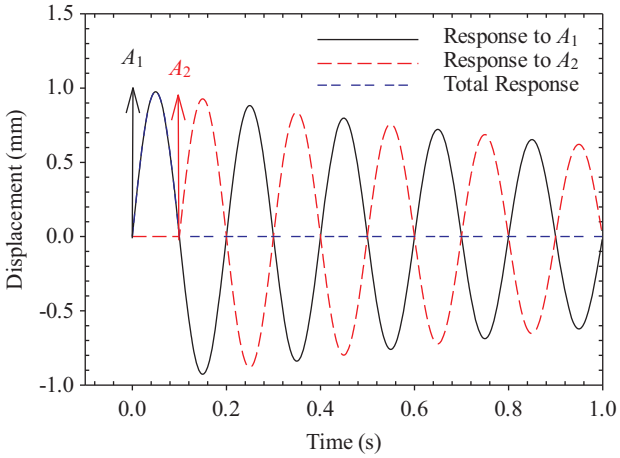

Fig. 1. Input shaping example of using two discrete input impulses to self-eliminate system vibration.

In the foregoing equation, the Heaviside unit step function is defined as follows (Mohammad, 2012):

$$u(t - t_2) = \begin{cases} 0, \; as \; t < t_2 \\ 1, \; as \; t \geq t_2 \end{cases}$$

The following constraint should be complied (here $m = 2$):

$$\sum_{i=1}^{m} A_i = 1 \tag{3}$$

The sum of the total amplitude of input impulses should be 1. Fig. 2 indicates that three input shapers are available. The required duration between impulses ΔT and corresponding impulse magnitude A_i can be determined using the natural frequency ω_n and damping ratio ζ of the system vibrational response (Singer, 1988). The detailed equations can be written as follows:

$$K = e^{-\frac{\pi\zeta}{\sqrt{1-\zeta^2}}} \tag{4}$$

$$\Delta T = \pi / \omega_n \sqrt{1 - \zeta^2} \tag{5}$$

Fig. 3 presents an example of using ZVD input shaping in the generation of a shaping command for three input impulses at three time points. An initial command is coupled with the input shaper to generate the final shaped command (Singer, 1988). Three impulses at different time instants are coupled with the initial command $r(t)$ to obtain the shaped command $r_{shp}(t)$. The input shaping technique aims to determine improved impulse magnitudes (A_1, A_2, A_3, …) and timing instants (t_1, t_2, t_3, …) for yielding the result depicted in Fig. 1. The higher number of impulses can improve vibration suppression at the expense of longer settling time. The time duration between the impulses of a ZD shaper is equal to one half period of vibration that lacks

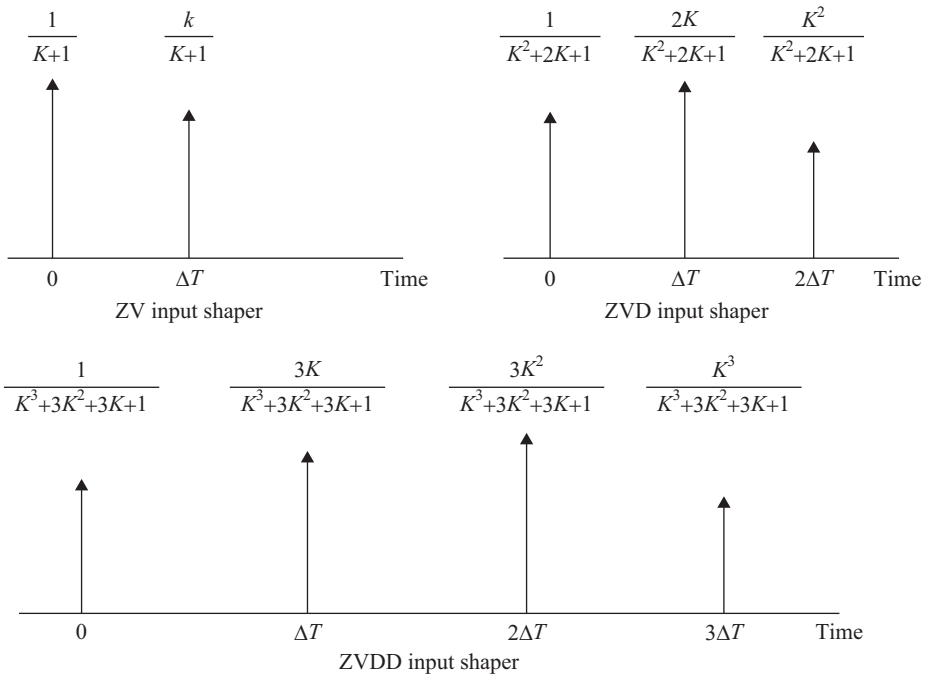

Fig. 2. Schematics of amplitudes and time intervals for ZV, ZVD, and ZVDD input shaper functions.

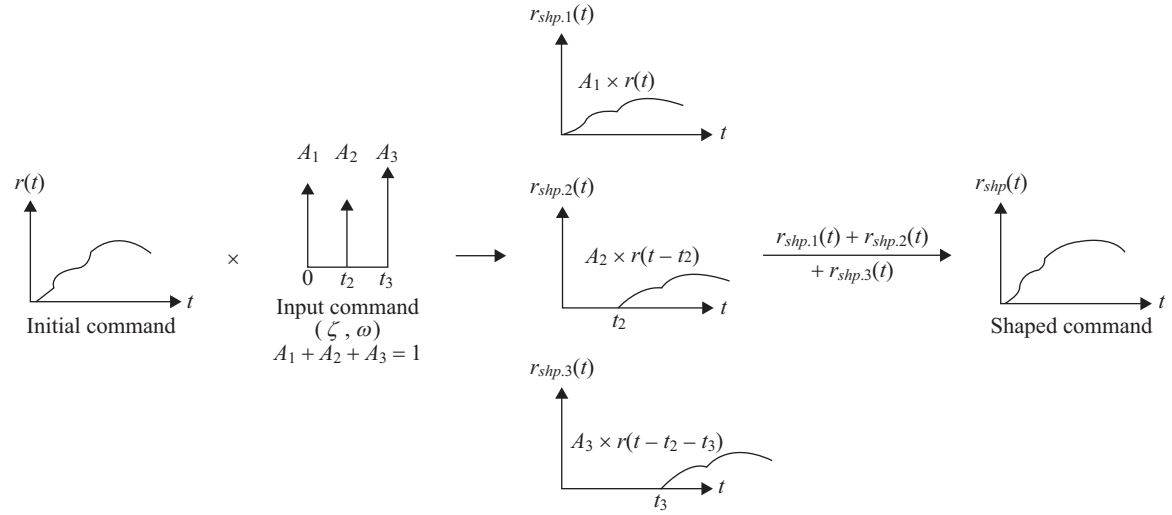

Fig. 3. ZVD input shaping used to generate shaping command for three input impulses at three time points.

robustness when the modeled, and actual parameters of the system are mismatched. To determine the duration between impulses and the corresponding impulse magnitude of the input shaper, knowledge regarding system characteristics is required. The EKF is introduced in the subsequent session as an automatic tuning method for input shapers.

2. Extended Kalman Filter

1) Kalman Filter

A KF combines the least square method and state-space representation in the recursive solution of linear filtering for a dynamic system. The KF is one of the optimal recursive algorithms in data processing, particularly in the field of navigation, communication, and satellite and flight control, where high tolerance to noise is crucial. Contrary to the ordinary concept of low-pass, high-pass, and band-pass filters, the KF is an estimation and prediction approach based on a probability density function. The KF, with the optimal recursive data processing algorithm, can estimate the present state by estimating the previous step and observing the current state. Therefore, without adopting previous observations and estimation data, less memory space

is used, and a shorter system response time can be obtained. Furthermore, the KF outperforms its low- and high-pass counterparts in handling probabilistic noises.

During execution, operations of the KF can be divided into two parts, namely prediction and correction. In the recursive process, the following notations are employed (Kovvali, 2013):

$\tilde{x}_k$: posteriori estimate vector at time step k
A_k: state transition matrix at time step k, $A \in R^{n\times n}$
B_k: input control matrix at time step k, $B \in R^{n\times 1}$
z_k: measurement vector at time step k
H_k: measurement matrix at time step k
v_k: measurement noise at time step k
Q_k: process noise covariance matrix
R_k: measurement noise covariance matrix
Q_k and R_k are the influences of the external disturbance noise and measurement noise, respectively, on the system. The recursive process of the KF can be explained as follows:

Prediction

State prediction:

$$\tilde{x}_k^- = A_k \tilde{x}_{k-1} + B_k u_{k-1} \tag{6}$$

Error covariance matrix prediction:

$$P_k^- = A_k P_{k-1} A_k^T + Q_k \tag{7}$$

Correction

State correction:

$$K_k = P_k^- H_k^T (H_k P_k^- H_k^T + R_k)^{-1} \tag{8}$$

$$\tilde{X}_k = \tilde{x}_k^- + K_k (z_k - H_k \tilde{x}_k^-) \tag{9}$$

$$P_k = (1 - K_k H_k) P_k^- \tag{10}$$

In the aforementioned procedure, estimation and prediction using the previous time step can be employed for estimating and predicting the subsequent time step; that is, the previous state is used to determine the subsequent state.

2) Extended Kalman Filter

The EKF is used in a nonlinear system to predict the state of the system. This system state modeling can be given as follows (Yazdanian, 2015):

$$x_k = f(x_{k-1}) + v_k \tag{11}$$

$$y_k = h(x_k) + w_k \tag{12}$$

where f and h denotes a state transition function and measurement function, respectively. v_k and w_k are noises. If f and h are differentiable, the Jacobian matrix can then be asymptotically employed to obtain a linearized model:

$$\tilde{F}_k = \frac{\partial f}{\partial x}\Big| m_{k-1|k-1} = \begin{bmatrix} \frac{\partial f_1}{\partial x_1} & \cdots & \frac{\partial f_1}{\partial x_{D1}} \\ \vdots & \ddots & \vdots \\ \frac{\partial f_D}{\partial x_1} & \cdots & \frac{\partial f_D}{\partial x_D} \end{bmatrix} \Big| m_{k-1|k-1} \tag{13}$$

$$\tilde{H}_k = \frac{\partial h}{\partial x}\Big| m_{k-1|k-1} = \begin{bmatrix} \frac{\partial h_1}{\partial x_1} & \cdots & \frac{\partial h_1}{\partial x_{D1}} \\ \vdots & \ddots & \vdots \\ \frac{\partial h_D}{\partial x_1} & \cdots & \frac{\partial h_D}{\partial x_D} \end{bmatrix} \Big| m_{k-1|k-1} \tag{14}$$

$m_{k-1|k-1}$ denotes the mean of Gaussian posterior state distribution at time step $k-1$, which is computed using measurements up to time step k. Thus, during the recursive process of the KF, Eqs. (6)-(10) can be given as follows:

Prediction

State prediction:

$$\tilde{m}_k^- = f(\tilde{m}_{k-1}) \tag{15}$$

Error covariance matrix prediction:

$$P_k^- = \tilde{F}_k P_{k-1} \tilde{F}_k^T + Q_k \tag{16}$$

Correction

State correction:

$$K_k = P_k^- \tilde{H}_k^T (\tilde{H}_k P_k^- \tilde{H}_k^T + R_k)^{-1} \tag{17}$$

$$\tilde{m}_k = \tilde{m}_k^- + K_k (z_k - \tilde{H}_k \tilde{m}_k^-) \tag{18}$$

$$P_k = (I - K_k \tilde{H}_k) P_k^- \tag{19}$$

3. Experimental Techniques

At time step k, assume that a decaying vibration signal has an amplitude of A and attenuation coefficient σ with sampling frequency f_s (Yazdanian, 2015):

$$s(k) = A e^{-\sigma \frac{k}{f_s}} \sin(\omega \frac{k}{f_s} + \varphi) \tag{20}$$

and the measured signal is as follows:

$$y_k = s(k) + n_k \tag{21}$$

where n_k denotes measurement noise. Because the EKF is used for state prediction, Eq. (20) can be expressed as follows:

$$\begin{aligned} s(k+1) &= Ae^{-\sigma\frac{k+1}{f_s}}\sin(\omega\frac{k+1}{f_s}+\varphi) \\ &= Ae^{-\frac{\sigma}{f_s}}\left\{\cos(\varphi)\left[e^{-\sigma\frac{k}{f_s}}\sin(\frac{\omega k}{f_s})\cos(\frac{\omega}{f_s})+e^{-\sigma\frac{k}{f_s}}\cos(\frac{\omega k}{f_s})\sin(\frac{\omega}{f_s})\right]\right. \\ &\left.+\sin(\varphi)\left[e^{-\sigma\frac{k}{f_s}}\cos(\frac{\omega k}{f_s})\cos(\frac{\omega}{f_s})-e^{-\sigma\frac{k}{f_s}}\sin(\frac{\omega k}{f_s})\sin(\frac{\omega}{f_s})\right]\right\} \end{aligned} \tag{22}$$

The state variables are subsequently defined as follows:

$$\begin{aligned} x_{1,k} &= Ae^{-\sigma\frac{k}{f_s}}\sin(\frac{\omega k}{f_s}) \\ x_{2,k} &= Ae^{-\sigma\frac{k}{f_s}}\cos(\frac{\omega k}{f_s}) \\ x_{3,k} &= \omega \\ x_{4,k} &= \sigma \end{aligned} \tag{23}$$

In the foregoing equations, $x_{i,k}(i = 1, 2, 3, 4)$ are the in-phase signal, quadrature signal, frequency, and damping ratio, respectively. According to Eqs. (21) and (22), the following state-space model can be derived:

$$\begin{aligned} x_{1,k+1} &= e^{-\frac{x_{4,k}}{f_s}}\left[x_{1,k}\cos(\frac{x_{3,k}}{f_s})+x_{2,k}\sin(\frac{x_{3,k}}{f_s})\right]+\omega_{1,k} \\ x_{2,k+1} &= e^{-\frac{x_{4,k}}{f_s}}\left[-x_{1,k}\sin(\frac{x_{3,k}}{f_s})+x_{2,k}\cos(\frac{x_{3,k}}{f_s})\right]+\omega_{2,k} \\ x_{3,k+1} &= x_{3,k}+\omega_{3,k} \\ x_{4,k+1} &= x_{4,k}+\omega_{4,k} \end{aligned} \tag{24}$$

where $\omega_{i,k}(i = 1, 2, 3, 4)$ is process noise (Yazdanian, 2015). The following equation is obtained by substituting a state-space model, that is, Eq. (24), into Eq. (21):

$$y_k = x_{1,k}\cos(\varphi) - x_{2,k}\sin(\varphi) + n_k \tag{25}$$

From Eq. (12), the measurement matrix can be written as follows:

$$H_k = \begin{bmatrix}\cos(\varphi) & \sin(\varphi) & 0 & 0\end{bmatrix} \tag{26}$$

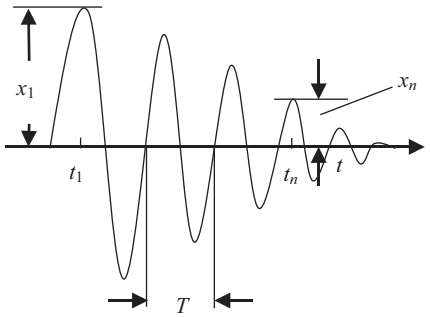

Fig. 4. Vibration signal with decaying amplitude over time.

With the obtained state-space model and measurement matrix, the EKF can be employed for predicting the vibration signal parameters.

For example, to obtain the damping ratio of a vibration signal in Fig. 4, vibration amplitudes x_1 and x_n respectively measured at t_1 and t_n can be calculated using Eq. (30), where ω_d, ω_n, and n are the damped natural frequency, natural frequency, and number sequence, respectively.

$$x(t) = Ae^{-\zeta\omega_n t}\sin(\omega_d t + \varphi) \tag{27}$$

and

$$\omega_d = \omega_n\sqrt{1-\zeta^2} \tag{28}$$

then

$$\frac{x_1}{x_n} = \frac{e^{-\zeta\omega_n t_1}}{e^{-\zeta\omega_n[t_1+(n-1)T]}} = e^{(n-1)\zeta\omega_n T} \tag{29}$$

$$\begin{aligned} In\frac{x_1}{x_n} &= (n-1)\zeta\omega_n T \\ &= (n-1)\zeta\omega_n\frac{2\pi}{\omega_d} \\ &= \frac{2\pi\zeta(n-1)}{\sqrt{1-\zeta^2}} \end{aligned} \tag{30}$$

The damping ratio ζ can be given as follows (Ogata, 1992):

$$\zeta = \frac{\frac{1}{n-1}(In\frac{x_1}{x_n})}{\sqrt{4\pi^2+[\frac{1}{n-1}(In\frac{x_1}{x_n})]^2}} \tag{31}$$

III. RESULTS AND DISCUSSION

MATLAB software was employed in this study for the dy-

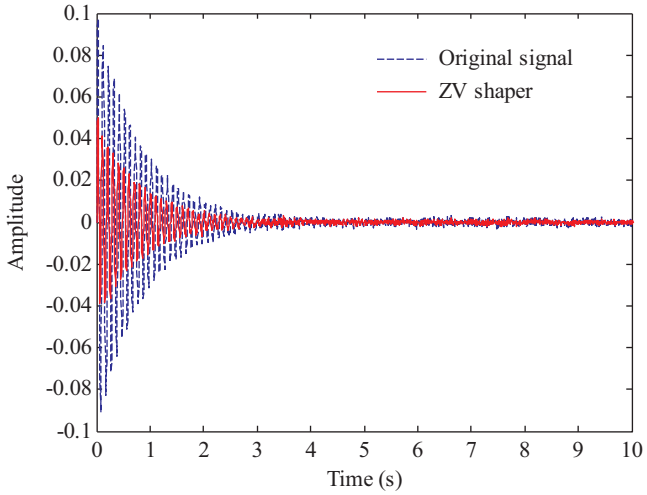

Fig. 5. Controlled response using EKF-ZV with initial frequency of 50 rad/s.

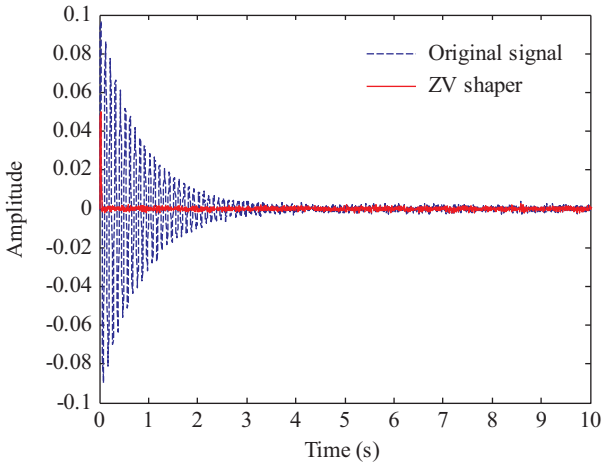

Fig. 6. Controlled response using EKF-ZV approach with initial frequency of 60 rad/s.

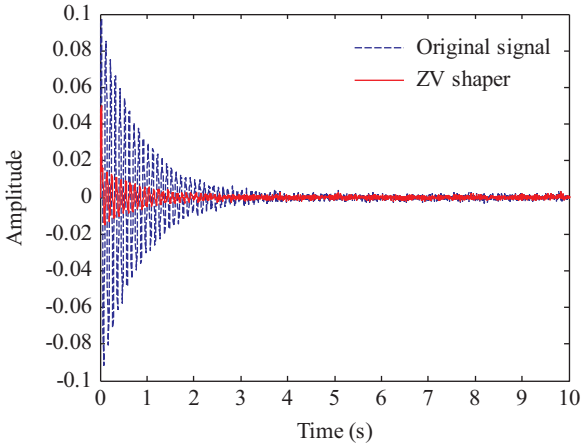

Fig. 7. Controlled response using EKF-ZV approach with initial frequency of 70 rad/s.

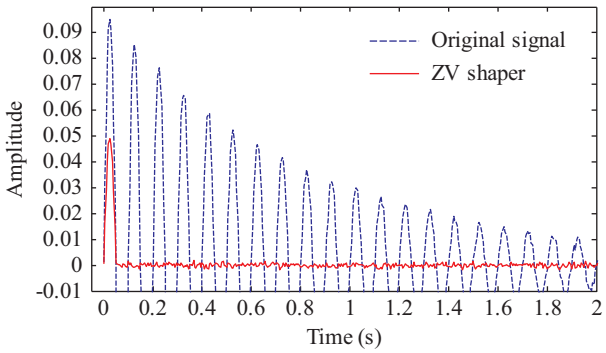

Fig. 8. Initial uncontrolled vibration response (blue) and vibration controlled using EKF-ZV input shaping (red).

namic simulation of the proposed technique. The parameters for frequency tracking and damping factor of the used EKF were first adjusted. The system was assumed to have an original free vibration response of 10 Hz (i.e., 62.8 rad/s) with an exponential decay time constant of 1.2 s. Thus, the initial frequency used in EKF was set at 50, 60, and 70 rad/s for comparing its influence. The covariance of the state estimation noise Q and the covariance of the measurement noise R are set as $10^{-2}\,\mathbf{I}_{4\times4}$ and 10^{-3}, respectively.

Fig. 5 presents the comparison between the original vibration response and that with the EKF-ZV approach. The effect of vibration suppression caused by the use of the EKF-ZV approach is evidently observed. The maximum calculated damping ratio is 0.08734. With the decay of the vibration signal, the damping ratio decreased accordingly.

When the initial test frequency was raised to 60 rad/s but close to 62.8 rad/s, Fig. 6 shows results with improved vibration suppression than its 50 rad/s counterpart. The calculated damping ratio increased to 0.7637. Fig. 7 presents the results with a further increase in the initial frequency to 70 rad/s. Although the vibration suppression effect was worse than that for 60 rad/s, it was superior to that for 50 rad/s. The damping ratio was reduced to 0.2054. An increase in damping ratio was observed when frequency tracking was close to ring-down signals. Fig. 1 indicates that input impulses A_1 and A_2 have a time lag of 0.1 s. The theoretical realization indicates remnant vibration caused by A_2 after vibrations excited by A_1 are damped out. However, decayed vibration is observed for small amplitudes (less than 10^{-7}). The influence of this remnant vibration is negligible.

After verifying the effectiveness of the EKF in parameter estimation, simulation was moved to the effect of different input shaping functions on vibration suppression. Figs. 8-10 present the results with ZV, ZVD, and ZVDD input shaping, respectively. The inset in each figure is local magnification at the beginning of the vibration response. For a quantitative comparison, settling time was defined as time required to reduce the vibration amplitude to 3% of the initial magnitude. These figures indicate the effectiveness of the proposed input shaping technique in vibration suppression. Table 1 summarizes performances of the proposed technique incorporating different input shaping

Table 1. Performances of the proposed control method.

Input shaper	Max. vibration amplitude	Settling time	Damping ratio
None	0.0970	2.925	0.0191
ZV	0.0498	0.075	0.6090
ZVD	0.0264	0.125	0.7611
ZVDD	0.0249	0.175	0.8759

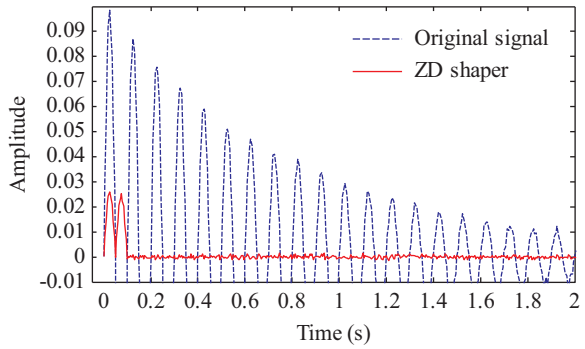

Fig. 9. Initial uncontrolled vibration response (blue) and vibration controlled with EKF-ZVD input shaping (red).

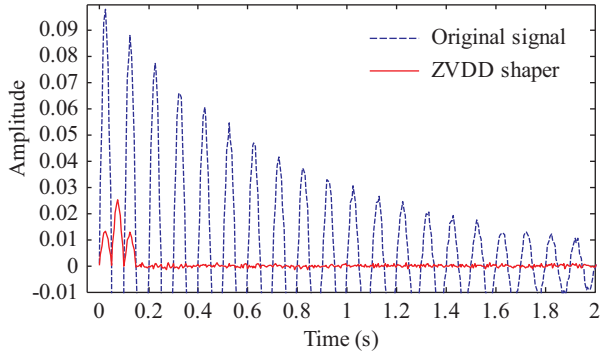

Fig. 10. Initial uncontrolled vibration response (blue) and vibration controlled using EKF-ZVDD input shaping (red).

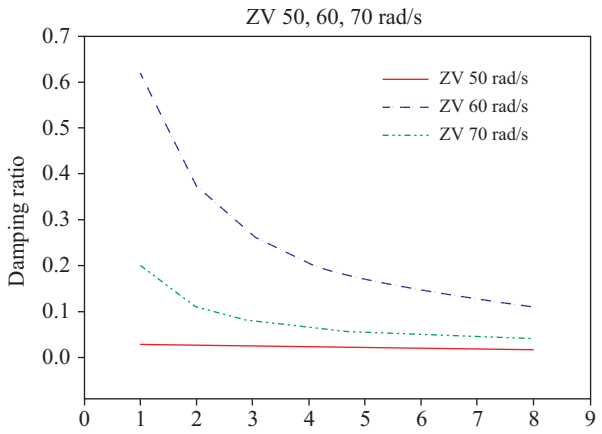

Fig. 11. Damping ratio of mismatch frequency obtained using ZV shaper with consecutive damped amplitude.

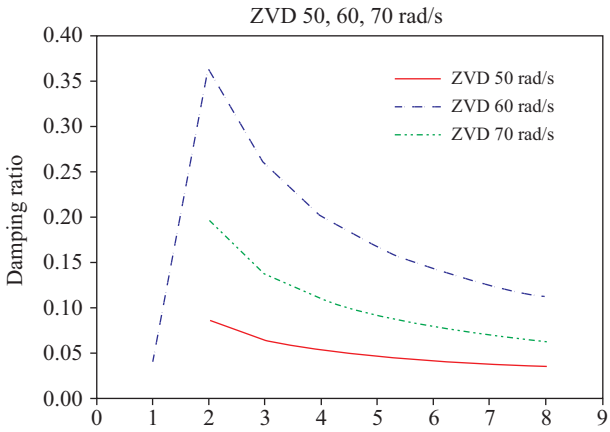

Fig. 12. Damping ratio of mismatch frequency obtained using ZVD shaper with consecutive damped amplitude.

functions. The maximum vibration amplitude reduces with the increasing number of input impulses used in input shaping. Nonetheless, settling time increases accordingly. This inhibits the evaluation of performance by using these two measures. Therefore, the damping ratio was adopted as a factor for evaluating vibration suppression performance. According to the control theory, the system with critical damping ($\zeta = 1$) generally demonstrates rapid settling without overshooting. Among the three input shaping functions, ZVDD provided a damping ratio that was closest to 1 and was considered the optimal input shaping function.

Figs. 11-13 compare the damping ratio curves of different mismatch frequencies for EKF-ZV, EKF-ZVD, and EKF-ZVDD shapers with consecutive, damped amplitudes. X-axis is numbered as 1, 2, …8 when the initial amplitude x_1 is divided using the consecutive damped amplitude $x_{n\text{-}1}$, with $n = 2, 3, \ldots 9$. The damping ratio in Figs. 11-13 are presented in Tables 2-4, 5-7, and 8-10, respectively. The amount of damping ratio decreases in Fig. 11 regardless of mismatch frequency estimation by the EKF. The sensitivity curves for the mismatch frequency are improved with the improving damping ratio when the frequency parameter modeled using the EKF is close to 62.8 rad/s. The damping ratio in each figure is calculated using Eq. (31) with the first vibration amplitude divided by the residual vibration amplitude. The first damping ratio in Fig. 12 first abruptly increases and then gradually reduces thereafter. This phenomenon is observed because the first suppressed vibration amplitude is

Table 2. ZV 50.

	X_1	X_2	X_3	X_4	X_5	X_6	X_7	X_8	X_9
X_n	0.05005	0.0412	0.0365	0.0324	0.0287	0.0255	0.0226	0.0201	0.0178
ζ		0.0310	0.0251	0.0231	0.0221	0.0215	0.0211	0.0208	0.0206

Table 3. ZV 60.

	X_1	X_2	X_3	X_4	X_5	X_6	X_7	X_8	X_9
X_n	0.0498	3.5e-4	3.1e-4	2.75e-4	2.4e-4	2.16e-4	1.9e-4	1.74e-4	1.64e-4
ζ		0.6195	0.3747	0.2656	0.2071	0.1706	0.1453	0.1275	0.1130

Table 4. ZV 70.

	X_1	X_2	X_3	X_4	X_5	X_6	X_7	X_8	X_9
X_n	0.0496	0.01332	0.01181	0.0105	0.0093	0.00824	0.00731	0.00649	0.00575
ζ		0.2048	0.1135	0.0822	0.0665	0.0570	0.0505	0.0462	0.0428

Table 5. ZVD 50.

	X_1	X_2	X_3	X_4	X_5	X_6	X_7	X_8	X_9
X_n	0.02475	0.03241	0.00823	0.0073	0.00647	0.00574	0.0051	0.00452	0.004
ζ		-0.0429	0.0873	0.0647	0.0533	0.0465	0.0419	0.0387	0.0362

Table 6. ZVD 60.

	X_1	X_2	X_3	X_4	X_5	X_6	X_7	X_8	X_9
X_n	0.0281	0.0218	1.99e-4	1.76e-4	1.56e-4	1.39e-4	1.2e-4	1.09e-4	9.66e-5
ζ		0.0408	0.3668	0.260	0.2024	0.1668	0.1427	0.1253	0.1122

Table 7. ZVD 70.

	X_1	X_2	X_3	X_4	X_5	X_6	X_7	X_8	X_9
X_n	0.0256	0.0264	0.0021	0.00186	0.00165	0.00147	0.0013	0.00116	0.00102
ζ		-0.0029	0.1961	0.1384	0.1089	0.0911	0.0791	0.0706	0.0642

Table 8. ZVDD 50.

	X_1	X_2	X_3	X_4	X_5	X_6	X_7	X_8	X_9
X_n	0.0125	0.028	0.0151	0.00243	0.00215	0.0019	0.0017	0.0015	0.00133
ζ		-0.127	-0.0148	0.0867	0.0699	0.0598	0.0530	0.0482	0.0445

Table 9. ZVDD 60.

	X_1	X_2	X_3	X_4	X_5	X_6	X_7	X_8	X_9
X_n	0.01514	0.02469	0.0102	8.46e-6	7.5e-6	6.65e-6	5.9e-6	5.23e-6	4.64e-6
ζ		-0.0776	0.0318	0.3693	0.2899	0.2390	0.2039	0.1783	0.1589

Table 10. ZVDD 70.

	X_1	X_2	X_3	X_4	X_5	X_6	X_7	X_8	X_9
X_n	0.01339	0.02562	0.01175	3.31e-4	2.93e-4	2.6e-4	2.3e-4	2.05e-4	1.82e-4
ζ		-0.1027	0.0104	0.1927	0.1503	0.1245	0.1071	0.0947	0.0853

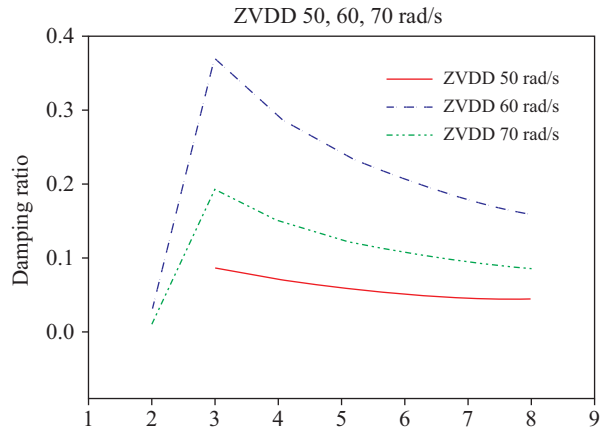

Fig. 13. Damping ratio of mismatch frequency obtained using ZVDD shaper with consecutive damped amplitude.

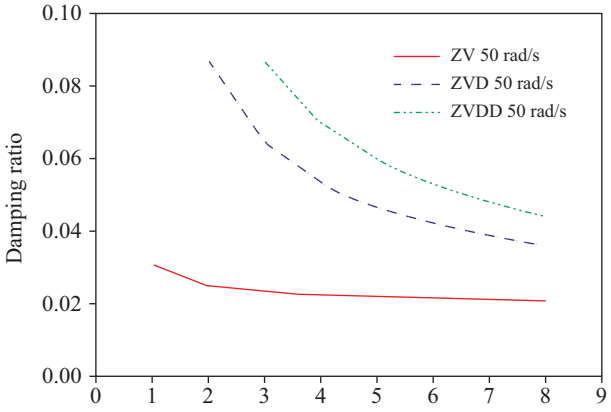

Fig. 14. Damping ratio of same mismatch frequency of 12.8 rad/s obtained using ZV, ZVD, and ZVDD shapers in consecutive damped amplitude.

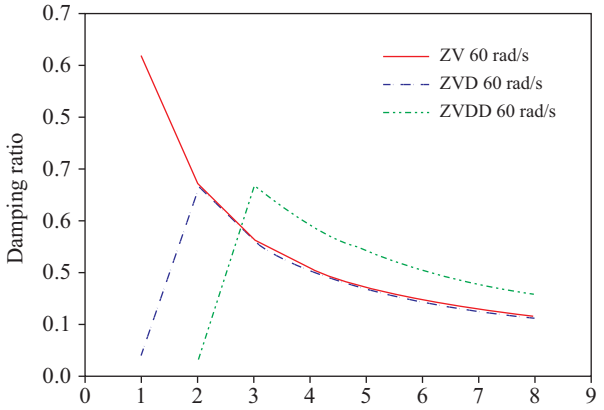

Fig. 15. Damping ratio of same mismatch frequency of 2.8 rad/s obtained using ZV, ZVD, and ZVDD shapers at consecutive damped amplitude.

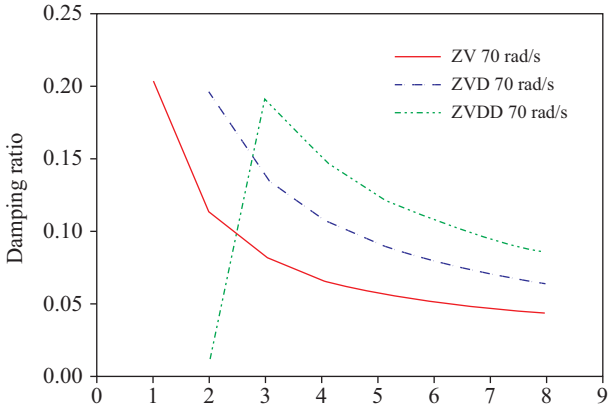

Fig. 16. Damping ratio of same mismatch frequency of 7.2 rad/s obtained using ZV, ZVD, and ZVDD shapers in consecutive damped amplitude.

less than the followed residual vibration amplitude, which was excited by the second impulse (Fig. 2). The consecutive imposed impulse amplitudes obtained using the ZVD and ZVDD approaches are higher than the first amplitude when they are adopted immediately after the first injecting impulse amplitude. Therefore, the damped amplitude in Eq. (31) provides an initial sharp curve, which is then followed by a gradually declining curve. The declining curve indicates the damping effect observed for ZV, ZVD, and ZVDD approaches. Only the positive damping ratio is plotted for the illustration of vibration suppression.

Figs. 14-16 compare damping ratio curves of the same mismatch frequency for 50, 60, and 70 rad/s by using EKF-ZV, EKF-ZVD, and EKF-ZVDD shapers. The amplitude of the first suppressed vibration is less than the followed subsequent vibration, which was excited by the second impulse, thus generating a negative damping ratio value. Because the consecutive (second) impulse amplitude imposed by ZVD and ZVDD are higher than the first amplitude when the shaper was adopted. Only the positive damping ratio is plotted for the illustration of vibration suppression. With the same mismatch frequency, the EKF-ZVDD approach provided improved suppression capability and was considered the optimal input shaping function. The aforementioned results were consistently deployed, although the initial covariance of state estimation noise Q and covariance of measurement noise R were increased by a factor ranging from 10^{-2} to 10^{2}.

To verify the vibration suppression of an EKF-IS model for mixed signals, a mixed frequency input signal with sampling frequency f_s of 10 Hz and the EKF frequency of 60 rad/s ($2\pi f$) are expressed as follows:

$$\begin{aligned} s(k) = 0.5 \times Ae^{-\sigma \frac{k}{f_s}} \sin(2\pi f \frac{k}{f_s} + \varphi) + 0.5 \\ \times Ae^{-\sigma \frac{k}{f_s}} \cos[2\pi(f+1)\frac{k}{f_s} + \varphi] \end{aligned} \quad (32)$$

The results obtained using ZV, ZVD, and ZVDD input shaping show that the EKF-IS controller exhibits satisfactory vibration suppression performance for mixed frequency signals. For example, the ZVDD has approximately zero vibration suppres-

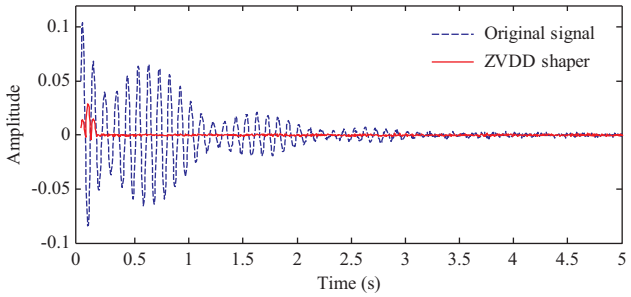

Fig. 17. Initial mixed error signal (blue) and error response obtained using EKF-ZVDD input shaping (red).

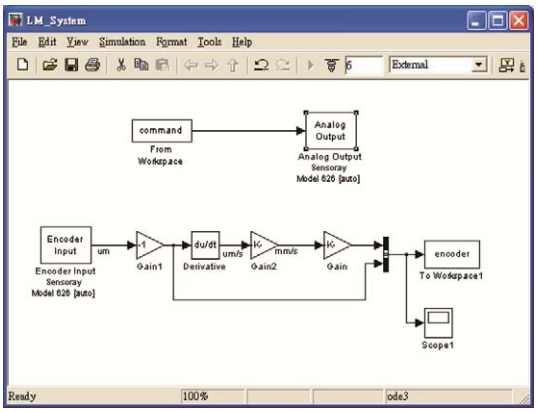

Fig. 18. Signal acquisition block diagram for the LSM experiment.

sion at 0.5 s (Fig. 17).

IV. EXPERIMENTAL RESULTS

Fig. 18 presents the setup of a single-axis linear synchronous motor (LSM). The adopted LSM is forced using a three-phase Y-connected two pole with the following parameters 1.5 kW, 60 Hz, 110 V, and 10.2 A. The motor is driven by a position-controlled analog voltage source inverter. The LSM is implemented using an intelligent-Xenus™ power component (XSL-230-40) manufactured by Copley controls Corp. The closed-loop feedback signals corresponding to LSM displacement can be measured using a linear encoder sensor (made by Renishaw-RGH41X50D05A). When the linear encoder sensor moves along an optical scale, it detects displacement and generates an output signal equivalent to that of an incremental encoder (Huang, 2014). A digital signal controller manufactured by Sensoray model 626 as a multifunction input/output card is used to validate the proposed EKF-IS system in practical applications. Here, this controller is termed model 626. The model 626 card is used to control real-time LSM motion. All experimental computer programs were conducted using MATLAB®/Simulink embedded in a PC-based development card.

Fig. 18 presents a MATLAB®/Simulink signal acquisition block diagram to obtain the transfer function of the LSM. A chirp control signal was used as an input command to the liner motor driver through an axis card. The output signal was captured using a linear encoder optical scale. Therefore, the frequency response of the LSM can be completed using the System Identification toolbox in MATLAB from the input control and output positioning signals.

Fig. 19. LSM with L-shaped iron plate.

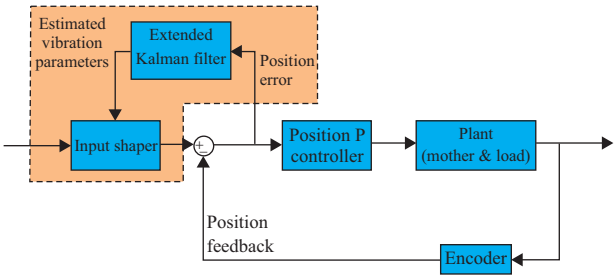

Fig. 20. EKF-IS control on LSM.

The identified continuous transfer function of the LSM is expressed as follows:

$$\frac{0.003346s^4+0.0108s^3\text{-}885.1s^2\text{-}1.224\times10^5s+9.687\times10^7}{s^4+76.17s^3+4.944\times10^4s^2+2.822\times10^6s+1.016\times10^8} \quad (33)$$

In the beginning, the positioning phenomena of the LSM in experimentation were hard to observe the vibration when there is no payload. An L-shaped iron plate was attached to the side of an LSM platform (Fig. 19). Fig. 20 presents the schematic of the proposed vibration suppression scheme in experiments.

Fig. 20 indicates that a reference position command was fed into the input shaper, and the position feedback was obtained from the linear optical encoder scale. The implemented EKF associated with the input shaper changes the new input command to the existing feedback control system. The position error subjected to an exponential decaying error signal is suppressed using the developed vibration suppression control as shown in the control block diagram. To verify the effect of the vibration suppression control, the LSM speed control command is set to 5 (mm/s) for 1 s. Figs. 21-23 present the vibration suppression performance of the LSM obtained using the EKF-IS with ZV, ZVD, and ZVDD schemes respectively. Different input shapers with low, high and low amplitudes in Fig. 2 create positive or negative damping effects. The input shaping signals generate

Table 11. Amplitude and damping ratio with EKF-ZV/ZVD/ZVDD

ZV	X_1	X_2	X_3	X_4
X_n	0.0549	0.05188	0.04046	0.0302
ζ		0.009	0.02428	0.03169
ZVD	X_1	X_2	X_3	X_4
X_n	0.04374	0.03699	0.02008	0.01092
ζ		0.02667	0.06184	0.07342
ZVDD	X_1	X_2	X_3	X_4
X_n	-0.06394	-0.03651	-0.01923	-0.002322
ζ		0.08883	0.09518	0.17323

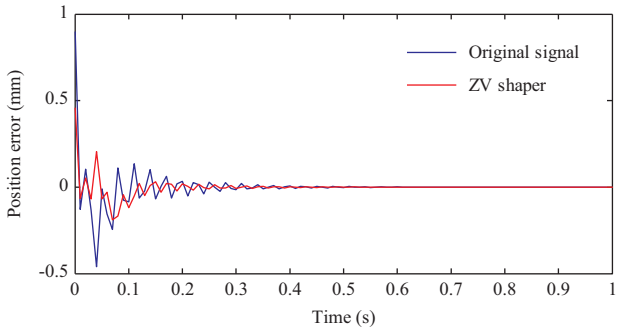

Fig. 21. LSM positioning error and result of vibration suppression signal with EKF-ZV.

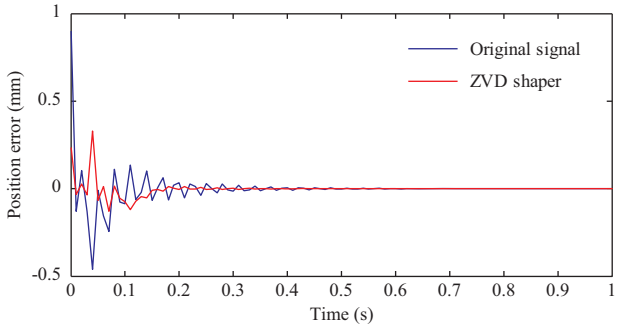

Fig. 22. LSM positioning error and result of vibration suppression signal with EKF-ZVD.

the initial transient response with positive and negative suppressed amplitude during error compensation. Therefore, Table 11 compares the amplitudes with damping ratio data for each input shaper after 0.1 s. Fig. 23 shows no vibration signal after 0.2 s for ZVDD. The amplitude of vibration is 0.03 mm for ZV and ZVD. Table 11 indicates that the damping ratio of ZVDD was higher than the others. Therefore, the vibration suppression performance of ZVDD is the optimal among the three input shapers. Nevertheless, the EKF-IS has an effect on real-time vibration suppression.

V. CONCLUSIONS

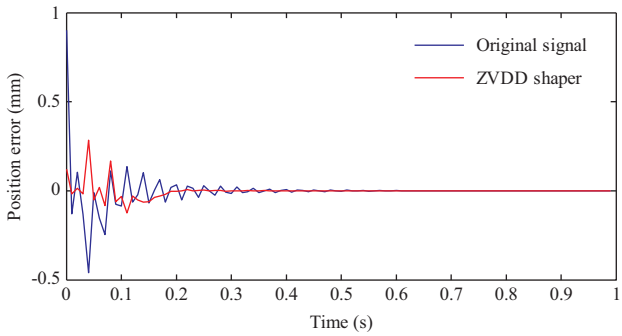

Fig. 23. LSM positioning error and result of vibration suppression signal with EKF-ZVDD.

In this study, different input shaping functions were used with the EKF for vibration suppression. The following conclusions were obtained:

(1) Compared with the uncontrolled vibration response signal, the proposed technique effectively reduces the amplitude and settling time of vibration.
(2) In the selection of an initial value for the EKF used in this study, although it was not the ideal value, the proposed technique demonstrated satisfactory vibration suppression.
(3) Among the three input shaping functions, the shaping function with a higher number of impulses exhibits the optimal suppression performance in terms of the vibration amplitude. Nevertheless, an increasing number of impulses increased the settling time for vibration suppression. On the basis of the damping ratio obtained in this study, input shaping with ZVDD exhibits the optimal performance in vibration suppression.
(4) From an in-lab single-axis linear motor experimentation, the EKF with ZVDD provides precise vibration control with an imported damping effect and low settling time.

VI. NOMENCLATURE

A_i Impulse magnitude
A_k State transition matrix at time step k, $A \in R^{n\times n}$
B_k Input control matrix at time step k, $B \in R^{n\times n}$

F_k	State transition Jacobian matrix at time step k
f	State transition function
f_s	Sampling frequency
H_k	Measurement matrix at time step k
$\tilde{H}_k$	State measurement Jacobian matrix at time step k
h	Measurement function
$InShp(t)$	Input shaping function
k	At time step k
$\tilde{m}_k^-$	Gaussian posterior mean at time step k
$m_{k-1\|k-1}$	Mean of Gaussian posterior state distribution at time step k −#1 computed using measurements up to time step k
n_k	Noise at time step k
P_k^-	Gaussian posterior covariance at time step k
Q_k	Gaussian state noise covariance at time step k
R_k	Gaussian measurement noise covariance at time step k
$r(t)$	Initial command
$r_{shape}(t)$	Shaped command at time step t
$s(k)$	Decaying vibration signal at time step k
t	Timing instants
u	Test input signal
$u(t-t_2)$	Unit step response function at time step t up to time step t_2
v_k	State transition noise at time step k
w_k	Measurement noise at time step k
x_n	Amplitude of vibration parameters
$\tilde{x}_k$	Posteriori estimate vector at time step k
y_k	Measured signal
z_k	Measurement vector at time step k
ΔT	Duration between impulses
δ	Dirac impulse function
ζ	Damping ratio
φ	Phase delay of impulse in shaping sequence
σ	Attenuation coefficient
ω_d	Damped natural frequency
ω_n	Natural frequency

ACKNOWLEDGEMENTS

The financial support from Ministry of Science and Technology under Grant No. MOST 105-2221-E-018-006 is gratefully acknowledged.

REFERENCES

Huang, Y. C. and Y. H. Li (2014). Experiments of iterative learning control system using particle swarm optimization by new bounded constraints on velocity and positioning. engineering computations 31(2), 250-266.

Huang, Y.-C., Y.-W. Su and P.-C. Chuo (2015). Iterative learning control bandwidth tuning using the particle swarm optimization technique for high precision motion. Microsystem Technologies 23(2), 361-370.

Kovvali, N., M. Banavar and A. Spanias (2013). An Introduction to Kalman Filtering with MATLAB Examples, Morgan and Claypool.

Longman, R. W., M. S. Chew and M. Q. Phan (2013). Precision motion control: intelligent mechanisms, morphing mechanisms. Lecture Notes in Electrical Engineering, Springer, 234. 1025-1033.

Mohammad R. K. (2012). Vibration Avoidance and Contour Error Compensation in High Speed Five-Axis Machine Tools Using Command Shaping Techniques, Master Thesis, The University of British Columbia, Vancouver, Canada.

Nuchkrua, T. and S. L. Chen (2017). Precision contouring control of five degree Robot Manipulator with uncertainty. International Journal of Advanced Robotic Systems, DOI: 10.1177/1729881416682703.

Ogata, K. (1992). System Dynamics, 2nd edition, Prentice Hall. 391-392.

Singer, N. C. (1988). Residual Vibration Reduction in Computer Controlled Machines. PhD Thesis, Department of Mechanical Engineering, MIT, The Artificial Intelligence Laboratory, Cambridge, Massachusetts, USA.

Singer, N. C. and W. P. Seering (1990). Preshaping command inputs to reduce system vibration. Journal of Dynamics System and Measurement Control 112(1), 76-82.

Singer, N. C. and W. P. Seering (1994). Residual vibration reduction using vector diagrams to generate shaped input. Journal of Mechanical Design, 116(2), 654-659.

Tsai, M. S., C. L. Yen and H. T. Yau (2017). Integration of input shaping technique with interpolation for vibration suppression of servo-feed drive system. Journal of the Chinese Institute of Engineers 40(4), 284-295.

Yoon, J., W. Bahn, T. Kim, J. Han, S. Lee and D. Cho (2015). A kalman-filter-based tuning method for input shapers in servo systems. Proceedings of 2015 International Automatic Control Conference (CACS), Yilan, Taiwan, Nov. 18-20.

Yazdanian, M., A. Mehrizi-Sani and M. Mojiri (2015). Estimation of electromechanical oscillation parameters using an extended kalman filter. IEEE Transaction on Power Systems 30(6), 2994-3002.